J Ther Eng, Vol. 12, No. 2, pp. 498−518, March, 2026

Journal of Thermal Engineering
Web page info: https://jten.yildiz.edu.tr
DOI: 10.14744/thermal.0001098

Research Article

Thermal performance evaluation of an underground U-bend tube heat exchanger integrated with phase change material

Md. Nur ALAM[1], Dipayan MONDAL[1,*], Mohammad Rafat ISLAM[1]

[1]*Department of Mechanical Engineering, Khulna University of Engineering & Technology, Khulna, 9203, Bangladesh*

ARTICLE INFO

Article history
Received: 19 December 2024
Revised: 07 April 2025
Accepted: 10 April 2025

Keywords:
Double U-shape Pipe; Ground Heat Exchanger; Numerical Simulation; Phase Change Material; Thermal Performance

ABSTRACT

This study presents a numerical investigation of the thermal performance of a U-bend tube ground heat exchanger (GHE) with paraffin wax as the phase change material (PCM) using ANSYS Fluent R1 2020. Using a U-tube instead of the straight tube results in the same or increased surface area at the reduced pipe length which further lowers the initial cost associated with GHE construction. Though there is a handful of studies regarding the performance enhancement of GHE, studies related to GHE with PCM, particularly fitted with a U-tube are inadequate, The GHE was constructed with a double U-shaped pipe, buried 45 meters underground, and the borehole was filled with paraffin wax as PCM due to its availability, steadiness, corrosion resistance, non-toxicity, and high latent heat capacity. The governing equations in this study are solved by the Realizable k-ε turbulence model. Air was circulated at velocities ranging from 0.5 ms^{-1} to 5 ms^{-1} in increments of 0.5 ms^{-1} for 12 hours to explore the system's performance, with an inlet temperature of 309 K in all cases. Upon increasing the velocity from 0.5 ms^{-1} to 5 ms^{-1}, it was found that at 12 hours of operation, the mean rate of heat transfer per meter increased from 76.27 Wm^{-1} to 116.45 Wm^{-1}, thus the highest velocity exhibiting a 65.5% increase over the lowest, while the temperature drop decreased as velocity increased, ranging from 9.09 °C at 0.5 ms^{-1} to 7.2 °C at 5 ms^{-1}. When it comes to effectiveness, initially for all air velocities the system's maximum effectiveness was found to be between 64% and 61%. After 12 hours, effectiveness dropped to 47% at 0.5 ms^{-1} and to 37% at 5 ms^{-1} demonstrating that effectiveness reduces over time and at lower velocities the system is more effective. Moreover, it was also found that after 40 meters of GHE, there was a minimal temperature change, thus using GHE beyond this length gives insignificant thermal benefits. This necessitates future research on finding the optimal length for GHE, focus should also be given to improving performance under various environmental conditions, design optimization, and thermal performance improvement, using phase change materials to reduce initial costs.

Cite this article as: Alam MN, Mondal D, Islam MR. Thermal performance evaluation of an underground U-bend tube heat exchanger integrated with phase change material. J Ther Eng 2026;12(2):498−518.

***Corresponding author.**
*E-mail address: dipkuet@me.kuet.ac.bd, dip.kuet@gmail.com

This paper was recommended for publication in revised form by Editr-in-Chief Prof. Dr. Ahmet Selim Dalkılıç

INTRODUCTION

Energy usage is increasing rapidly worldwide due to population growth and improved living conditions, leading to a rise in greenhouse gas emissions. Around 40% of the world's energy consumption is utilized in heating and cooling spaces [1]. Traditional HVAC systems are not sustainable and contribute to environmental pollution. Geothermal energy, found beneath our feet, can be harnessed for cooling and heating buildings [2], [3]. Soil temperature below the ground surface is consistent year-round, but comparatively higher in the cold season and lower in the hot season relative to ambient temperatures [4]. Ground heat exchangers (GHE) facilitate heat transfer with underground soil, by receiving heat during winter and by releasing the same during summer. These systems can be placed horizontally or vertically, and the conditioned air is to be used for cooling or heating the buildings [5], [6]. The longer pipelines and excavation costs increase initial investment. Also, increase soil wetness or use a backfilling material with higher heat conductivity than native soil to reduce pipe length. Kong et al. [7] studied the thermal behavior of the GSHP with various U-tube variant buried pipes experimentally and numerically, their findings reveal that smooth U-tubes performed better than petals. Pu et al. [8] explored a numerical study on vertical U-tube type heat exchangers for GSHP systems revealing that increasing U-tube diameter and Reynolds number enhances integrated performance. Jalaluddin et al. [9] compared the performance of various GHEs on a steel pile foundation, revealing that double-tube GHEs had the maximum heat transfer rate, while factors like soil type, operation duration, inlet temperature, and material also influenced performance. Liu et al. [10] used a transient 3D model in ANSYS FLUENT to explore the behavior of the EAHE system integrated with the PCM. Gao et al. [11] studied to evaluate pile-foundation heat exchanger efficiency for geothermal energy utilization in Shanghai, analyzing single, double, and triple U-shaped and W-shaped high-density Polyethylene-based ground-coupled heat exchangers (GCHE). Their study revealed that with a modest medium flow rate, the W-shaped configuration seems to be the most effective. Chen et al. [12], [13] examined how PCM grout affects ground source heat pump (GSHP) efficiency. The system efficiency improves with PCM grouts with equivalent thermal conductivity, especially in buildings with low thermal demand. Qi et al. [14] investigated to explore PCM usage as backfill in ground source heat pumps, emphasizing its benefits stemming from their minimal thermal impact radius and stable temperature. Ahmed et al. [15] explored the optimal performance of a HEPC system using the CFD simulation by considering the velocity of air at 1.5 ms^{-1} through the buried pipe of 60 m length, 0.062 m dia., 0.003 m thickness, and 8 m depth. Yang et al. [16] found that borehole ground heat exchangers with PCM backfill boost heat exchange rate, delay soil temperature variation, improve energy storage, and reduce soil thermal interference radius. Bottarelli et al. [17] conducted a test on shallow horizontal GHEs using PCMs to improve heat pump performance and prevent winter thermal depletion. Yusof et al [18] examined an EAHE technique using a laboratory simulator and found that a certain flow rate and ground temperature reduce temperature and transfer heat best. Li et al [19] developed a numerical representation of a horizontal spiral-coil GSHP system and examined performance aspects such as soil thermal conductivity and pipe spacing. Misra et al. [20] introduced EAHE to evaluate the thermal performance under unstable situations and found that transient conditions considerably affected the performance. Florides et al. [21] examined the efficiency of vertical and horizontal ground heat exchanger modeling. Their study revealed that, while working in identical conditions, vertical heat exchangers perform better than horizontal heat exchangers. Cui et al. [22] in their study, recommended a vertical over horizontal ground heat exchanger when it comes to both thermal performance and cost-effectiveness.

Ghosal et al. [23] introduced a MATLAB model to estimate the behavior of EAHE systems and analyze the impact of factors on greenhouse air temperatures which reveals that EAHE systems significantly increase winter temperatures by 7-8°C and lower summer temperatures by 5-6°C compared to a similar greenhouse without it. Morshed et al. [24] examined two EAHE setups in Basra Province (Iraq): dry soil and moist soil made artificially and found that wet systems had a higher average COP (6.41) than dry systems (5.07). Hsu et al. [25] studied an integrated system for earth-air heat exchangers in high-density housing, using water-filled raft foundations. Tested in Yilan, Taiwan, it showed similar cooling potential and lower construction costs than conventional EAHEs. Aditya et al. [26] compared GSHP and hybrid GSHP (HGSHP) systems' costs to conventional ones in various climatic conditions, revealing that the performance is influenced by factors such as ground conditions, meteorological conditions, drilling costs, power pricing, and gas pricing. Gao et al. [27] evaluated the operational capability of 26 GSHP systems in Sichuan, Chongqing, and Shaanxi, analyzing heat pump performance, water transfer factor, and energy efficiency ratio, and providing recommendations for improvement in system design, construction, and operation. Zhuo et al. [28] experimentally explored the effects of SSPCM used as backfill on borehole GHE systems. Their findings reveal that there is a considerable reduction in temperature variation by up to 10°C because of using SSPCM as backfill material, especially around the heat source. Zhang et al. [29] examined the thermal behavior of PCM-integrated LTHS through fin incorporation. They observed that, upon increasing the PCM's thermal conductivity by 0.2 $Wm^{-2} \cdot K$, there is a significant reduction in melting and solidification time of the PCM by 43% and 35 %. Moreover, it was also found that HTF velocity has a significant effect on heat exchanger efficiency compared to the fluid's temperature

and thermal conductivity of PCM. Emmi and Bottarelli [30] numerically studied the thermal capability of HGHE directly coupled with PCM. Results found show that coupling PCM directly with HGHEs performs better compared to using PCM added to the backfill material. Hadjadj et al. [31] experimentally investigated the effect of air speed on HWAHE performance. The authors discovered that as air velocity increased, efficiency trended downward. Han et al. [32] examined the thermal performance of a solar-coupled GSHP system in a large building, finding high efficiency but decreasing efficiency with increasing heat exchanger spacing. Zhou et al [33] developed a PCM-filled EAHE to minimize HVAC energy usage, increasing cooling capacity by 20.24% and lowering output temperature by 0.83°C. In addition, Mondal et al. [34], [35] conducted the parallel, counter, and cross-flow water-to-air u-bend heat exchanger and also a cooling system adopted by the vapor absorption system, while Mondal and Islam [36] reported another study for intermittent system adopted by ammonia absorption refrigeration system. To fit the refrigerants in HVAC&R systems, Mondal et al. and Islam et al. [37]–[41] measured the transport properties as well as the heat transfer characteristics of several refrigerants that will take in the future revolution of industries. Moreover, Das et al. [42] and Arefin et al. [43] assessed the thermodynamic analysis of the dual and single cascading vapor compression cycle, respectively, for the low-temperature application. Moreover, Bari et al. [44] presented the analysis of heat transmission in a refrigerant compartment, while Shahariar et al. [45] represented the performance of LiCl desiccant dehumidifier. Rifert et al. [46] studied several approaches for estimating heat transfer in horizontal and smooth pipes during condensation when vapor velocity is present. The authors suggested a semiempirical dependence $Nu = 0.0144Fr^{36}Pr^{0.43}$ to calculate condensation heat transfer when $Re > 800$ and β (A parameter responsible for governing vapor velocity) > 10. Rifert et al. [47] reviewed over 40 semi-empirical and empirical techniques to predict heat transfer coefficients in condensation processes within plain tubes. The authors concluded that during the condensation of various refrigerants, the correlations suggested by Thome et al. [48], Cavallini et al. [49], Shah [50], and Rifert et al. [51], [52] can be used to predict the heat transfer coefficients. Camaraza-Medina et al. [53] after comparing 22 different published experimental data of condensable fluid inside horizontal, vertical tubes, and inclined tubes, suggested a new model for heat transfer calculation during film condensation within pipes, good enough to be considered satisfactory for practical design.

From the above discussion, the thermal efficiency and pipe length of a ground heat exchanger are critical considerations in calculating excavation costs and soil volume requirements. Adding phase change material (PCM) may greatly increase thermal performance. PCM-filled GHEs improve summer cooling capacity by enhancing heat transfer and delaying the transition from heating to cooling mode, resulting in excellent cooling performance. PCM-air is more energy-efficient than PCM-water, making it a good choice for energy storage systems. Hence, by introducing PCM into the conventional ground heat exchanger system, a significant improvement may be obtained in thermal performance. Moreover, by utilizing a U-bent tube design instead of a traditional straight tube, the overall surface area of the GHE can either be maintained or even increased while simultaneously reducing the required length of the pipe. The reduction in pipe length contributes to a friendly and space-efficient system without compromising performance. Additionally, the pressure drop at the U-bent tube section is minimized compared to straight tubes, resulting in improved fluid flow dynamics, lower pumping power requirements, and further optimization of the system's energy efficiency. There are few studies on phase change material double U-shaped tube heat exchangers, which reduce pipe depth and improve GHE thermal performance. This simulation study examines the thermal performance of a U-tube ground heat exchanger with PCM as the backfill material buried under soil by varying air velocity ranging from 0.5 ms^{-1} to 5 ms^{-1}. A transient three-dimensional simulation model has been developed and analyzed numerically via FLUENT 2020 R1 to find the system's best design and operation characteristics.

MATERIALS AND METHODS

Assumption

A 3D domain has been introduced in the numerical model by encompassing a complex dynamic process of heat transfer that includes convective heat transfer, heat conduction, and PCM melting as well as solidification for the inside pipe, soil, and borehole, respectively. The specific assumptions are considered as follows:

- Thermophysical properties of air are assumed to be constant and incompressible.
- The soil around the borehole is homogeneous and isotropic with constant thermo-physical properties.
- PCM are assumed to have temperature-independent thermophysical properties.
- The physical contact of material layers is assured, and the thermal resistance of the pipe thickness and borehole is neglected.
- Air is assumed to mix uniformly inside the Ground Air Heat Exchanger (GAHE) pipe ensuring uniform temperature with no stratification.
- The heat transfer is modeled as transient and occurs in three dimensions through the surrounding soil.
- Apart from air velocity, all other parameters are assumed to be constant

Material

PCM is filled inside the borehole as backfill material around the pipe buried in the ground as part of the model.

Table 1. Thermophysical properties of air, soil, and paraffin wax [10] (The properties are taken at a reference temperature of 293.15 K)

Parameters	Value		
	Air	Soil	Paraffin wax
Density, kg/m^3	1.165	1700	800
Latent heat, J/kg	-	-	250×10^3
Melting Temperature, °C	-	-	25
Specific heat capacity, J/(kg.K)	1006	1300	3220
Thermal conductivity, W/(m.K)	0.0262	1.1	0.35
Viscosity, kg/(m.s)	1.8×10^{-5}	-	0.094

As a fluid for heat transmission, the surrounding air moves along the borehole's axis through the pipe. Paraffin was used as PCM to fill the gap between the borehole walls and the pipe. The properties of air, soil, and paraffin wax as PCM are listed below in Table 1. All the properties are taken at a reference temperature of 293.15 K.

Physical Model As Proposed Geometry

Figure 1 represents the schematic diagram of an underground heat transfer model with a vertical double U-tube ground heat exchanger (GHE) with inlet and outlet, phase change material (PCM), and ambient soil. The following displays both the orientation and the physical dimension.

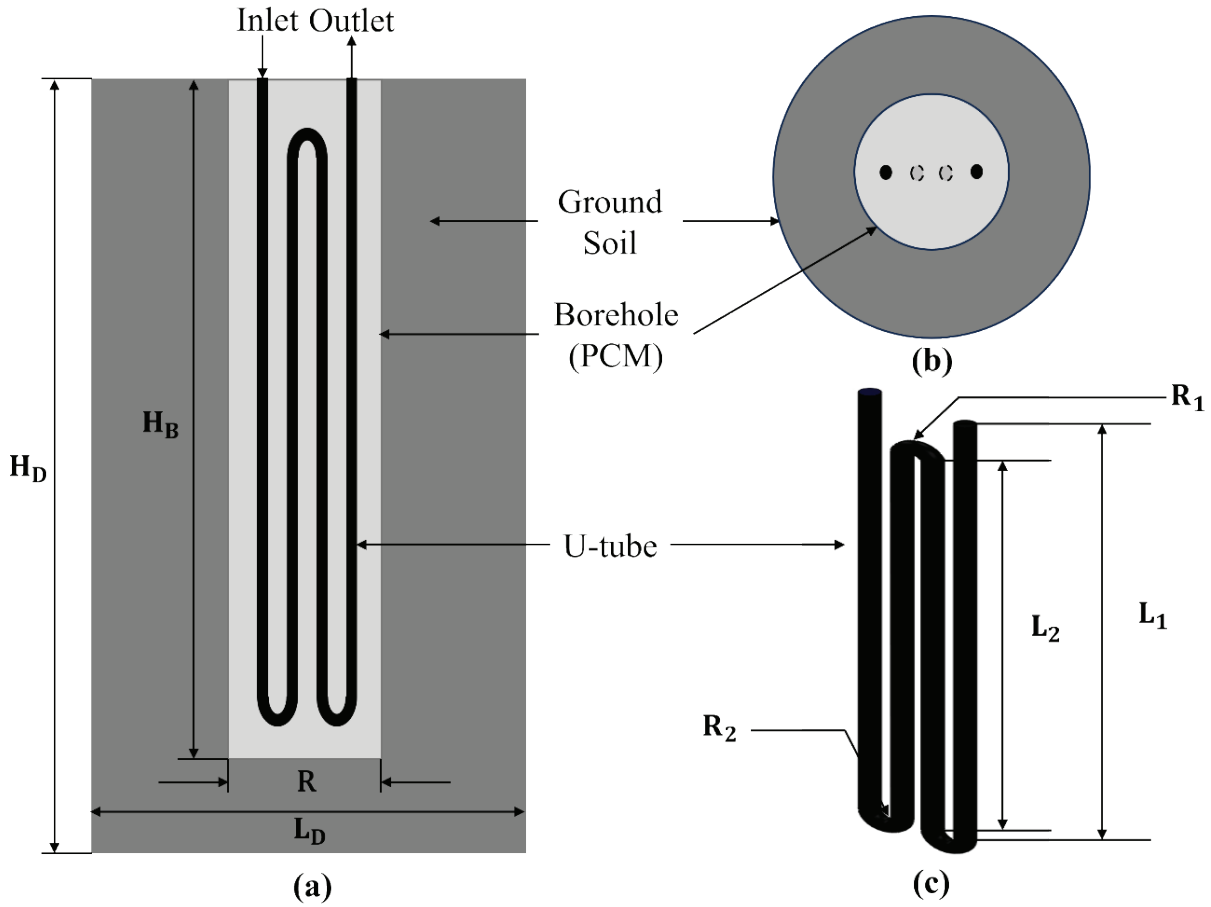

Figure 1. Schematic diagram of ground heat exchanger: (a) front view, (b) top view, and (c) tube geometry.

Table 2. The specifications of the proposed geometry

Parameters	Value	Parameters	Value
Domain length, L_D (m)	10	Tube radius, mm	16
Domain width, W (m)	5	Tube length, L_1 (m)	40
Domain height, H_D (m)	45	Tube length, L_2 (m)	39.65
Borehole height, H_B (m)	42	Tube bend radius, R_1 (mm)	57
Borehole radius, R (mm)	300	Tube bend radius, R_2 (mm)	25

Meanwhile, the specifications of the physical model are listed in Table 2.

Formation of the Problem

To simulate the study using ANSYS FLUENT, some governing equations were used that characterized the GHE's heat transfer and fluid movement. However, the governing equations [54] used for this study are described as:

The continuity equation is defined as,

$$\frac{\partial \rho_a}{\partial t} + \frac{\partial}{\partial x_i}(\rho_a u_i) = 0 \tag{1}$$

The momentum equation is defined as,

$$\frac{\partial}{\partial t}(\rho_a u_i) + u_j \frac{\partial}{\partial x_j}(\rho_a u_i) = -\frac{\partial p_a}{\partial x_i} + \eta_a \frac{\partial^2 u_i}{\partial x_j \partial y_j} \tag{2}$$

The energy equation is defined as,

$$\rho_a C_a \left(\frac{\partial T}{\partial t} + u_j \frac{\partial T}{\partial x_j}\right) = \frac{\partial}{\partial x_j}\left[(\lambda_a + C_a . \frac{\eta_t}{\sigma_T})\frac{\partial T}{\partial x_j}\right] \tag{3}$$

Where, ρ_a, P_a, η_a, and λ_a denote density, pressure, dynamic viscosity, and thermal conductivity of air, respectively. Again, x_i & x_j, and u_i & u_j represent the length and velocity components, respectively.

Turbulence model:

The 'Realizable k-ε turbulence model' is widely used to simulate GSHE systems due to its ability to produce reliable outcomes for confined wall internal flows with modest mean pressure gradients [55]. Hence this model is to be employed at transport equations as follows:

Transport equation for 'k';

$$\frac{\partial}{\partial t}(\rho k) + \frac{\partial}{\partial x_j}(\rho k u_j) = \frac{\partial}{\partial x_j}\left[\left(\mu \frac{\mu_t}{\sigma_k}\right)\frac{\partial k}{\partial x_j}\right] + G_k + G_b - \rho\varepsilon - Y_M + S_k \tag{4}$$

Transport equation for 'epsilon (ε)';

$$\frac{\partial}{\partial t}(\rho\varepsilon) + \frac{\partial}{\partial x_i}(\rho\varepsilon u_j) = \frac{\partial}{\partial x_j}\left[\left(\mu \frac{\mu_t}{\sigma_\varepsilon}\right)\frac{\partial \varepsilon}{\partial x_j}\right] + \rho C_1 S_\varepsilon - \rho C_2 \left(\frac{\varepsilon^2}{k + \sqrt{\nu\varepsilon}}\right) + \frac{\varepsilon}{k} C_1 C_{3\varepsilon} G_b + S_\varepsilon \tag{5}$$

Where,

$$C_1 = \max\left[0.43, \frac{\eta}{\eta + 5}\right]$$

$$\eta = S\frac{k}{\varepsilon}; S = \sqrt{2 S_{ij} S_{ij}}$$

$$\mu_t = \rho C_\mu \frac{k^2}{\varepsilon}$$

Where α_k and α_ε represent the Prandtl numbers for k and ε; μ_a and μ_t denote the dynamic viscosity and turbulent (or eddy) viscosity of air; G_k and G_b represent the turbulence-generated kinetic energy for the velocity gradients and buoyancy, respectively. Again, Y_M represents the dilatation dissipation rate, while S_ε & S_k denote the user-defined source terms. Also, the constants for the k-ε realizable model are listed as, $c_{1\varepsilon}$=1.44, c_2=1.90, σ_k=1.00, σ_ε=1.20.

Phase change model:

For modelling the solidification and melting of PCM grout, the enthalpy porosity approach was used. [56], [57]. The melt interface is not well traced by this method, which regards the liquid-solid mushy zone as a porous zone with the same porosity as the liquid fraction. This model uses the enthalpy balance to determine the liquid fraction at each iteration. The summation of sensible enthalpy (h) and the latent heat (ΔH) gives the total enthalpy [54]:

$$H = h + \Delta H \tag{6}$$

$$h = h_{ref} + \int_{T_{ref}}^{T} c_p . dT \tag{7}$$

$$\Delta H = \beta L \tag{8}$$

Where T_{ref} and h_{ref} represents the reference temperature and enthalpy respectively, and L denotes the PCM's latent heat. If PCM's melting and solidification temperatures are considered of T_{liquid} and T_{solid}, respectively, then the liquid fraction (β) is defined as:

$$\beta = \begin{cases} 0, & T < T_{solid} \\ \frac{T - T_{solid}}{T_{liquid} - T_{solid}}, & T_{solid} < T < T_{liquid} \\ 1, & T > T_{liquid} \end{cases} \tag{9}$$

The usual momentum equation should include a sink term to account for solid phase pressure drop:

$$S_{hj} = \frac{(1-\beta)^2}{\beta^3+\theta} A_{mush}\, u_j \quad (10)$$

Where θ denotes a small number (0.001) to avoid zero division; A_{mush} represents the mushy zone which measures the damping amplitude, varying from 10^4 to 10^7 which is considered as 10^5 for this study [58], [59].

Effectiveness:

The ratio of the actual drop in air temperature to the maximum possible drop in air temperature in in ground heat exchanger system is termed as effectiveness [18]. The equation below is applied to determine the effectiveness [60]:

$$\varepsilon = \frac{Actual\ Temperature\ Drop\ at\ Any\ Point\ of\ Time}{Maximum\ Possible\ Temperature\ Drop} = \frac{T_{ai}-T_{ao}}{T_{ai}-T_{w,initial}} \quad (11)$$

where, T_{ai} and T_{ao} are the inlet and outlet air temperature, and $T_{w,\ initial}$ is the initial temperature of the pipe wall.

Boundary conditions and solver setup

For the top surface, the energy balance of the soil surface is as follows [10]:

$$-\lambda_s\left(\frac{\partial T}{\partial y}\right)_{y=0} = CE - LR + SR \quad (12)$$

Here, CE refers to the heat transfer between the soil surface and surrounding air.

$$CE = h_{sur}(T_{amb} - T_{ss}) \quad (13)$$

Where, T_{amb} and T_{ss} represent the temperature of ambient air and soil surface, respectively; h_{sur} denotes the convective heat transfer coefficient of the soil surface which is estimated as follows [61]:

$$h_{sur} = \begin{cases} 5.678[0.775 + 0.35(\frac{v_{wind}}{0.304})], v_{wind} < 4.88 \\ 5.678[0.775 + 0.35(\frac{v_{wind}}{0.304})^{0.78}], v_{wind} \geq 4.88 \end{cases} \quad (14)$$

Where v_{wind} represents the velocity of air at the soil surface; LR denotes the soil surface emitted long-wave radiation which is expressed as:

$$LR = \epsilon \Delta R \quad (15)$$

Where ϵ(=1) is the ground surface emittance and ΔR is a quantity that is dependent on the soil radiative characteristics, the effective sky temperature, and the relative humidity of the ground and air above the ground surface. Here, ΔR= 63 W/m^2 [62]; may be used as the first approximation.

Again, the SR is the amount of solar radiation that the soil surface absorbs as:

$$SR = (1-\alpha)G \quad (16)$$

Where G and α represent the incident solar global irradiance and soil surface albedo. However, the following equations provide a good description of the radiation and convection heat transfer processes based on the explanation above [63]:

$$-\lambda_s\left(\frac{\partial T}{\partial y}\right)_{y=0} = h_{sur}(T_{sol-air} - T_{ss}) \quad (17)$$

$$T_{sol-air} = T_{amb} + \frac{(1-\alpha)G}{h_{sur}} - \frac{\epsilon \Delta R}{h_{sur}} \quad (18)$$

Where $T_{sol\text{-}air}$ defines the solar-air temperature. Beyond the boundary, the temperature of the soil at the bottom surface stays constant at the same level as the soil surface's mean yearly temperature. Therefore, it is seen as:

$$T(bottom, t) = 20℃ \quad (19)$$

For faraway surfaces, adiabatic conditions are used. The surrounding soil and pipe walls were coupled to facilitate heat transfer. However, a brief description of the boundary conditions is listed in Table 3.

The coupled technique was used to solve the pressure-velocity coupling in the solver configuration. Second-order and least square cell-based (LSCB) techniques were chosen for the solution of pressure and velocity gradients, respectively. For turbulent kinetic energy and momentum, the second-order upwind approach was used. When the residuals were less than those for energy and other variables, convergence was attained. A brief description of the solver setup is listed in Table 4.

Mesh Independence and Model Validation

ANSYS software 2020 R1 was used to generate the required mesh and a 3D non-uniform mesh was applied to the study. After the creation of geometry, the following mesh has been generated in ANSYS meshing of tetrahedrons type. Figure 2 illustrates the grid layout and provides an in-depth look at the borehole cross-section. The mesh independence test determines if the output is mesh-dependent for validation. An independence test is performed using three different grid sizes to ensure the precision of the proposed work's simulated outcomes. The temperatures

Table 3. Brief description of the boundary conditions

Items		Description
Top surface		Wall (Convection)
Bottom surface		Wall (Temperature)
		Temperature specified at 288 K
Faraway surface		No-slip wall (Heat flux)
Inlet	: Inlet	Velocity-inlet
	: Temperature (T)	309 K
	: Velocity (v)	0.5 ~ 5 m/s
Outlet		Pressure-outlet
Other walls		No-slip, coupled wall
Initial temperature for all zones (T)		288 K

Table 4. Brief description of the solver setup

Item	Description	
Solver type	Pressure Based Solver	
Condition	Transient	
Gravity	On	
Turbulence model	k-ε (K-Epsilon),	
Near wall treatment	Standard wall functions	
Solver method	Pressure-velocity coupling: Coupled	
Initialization	Standard initialization	
Spatial Discretization	Gradient	Least square cell based
	Pressure	Second order
	Momentum	Second-order upwind
	Turbulent kinetic energy and dissipation rate	First order upwind

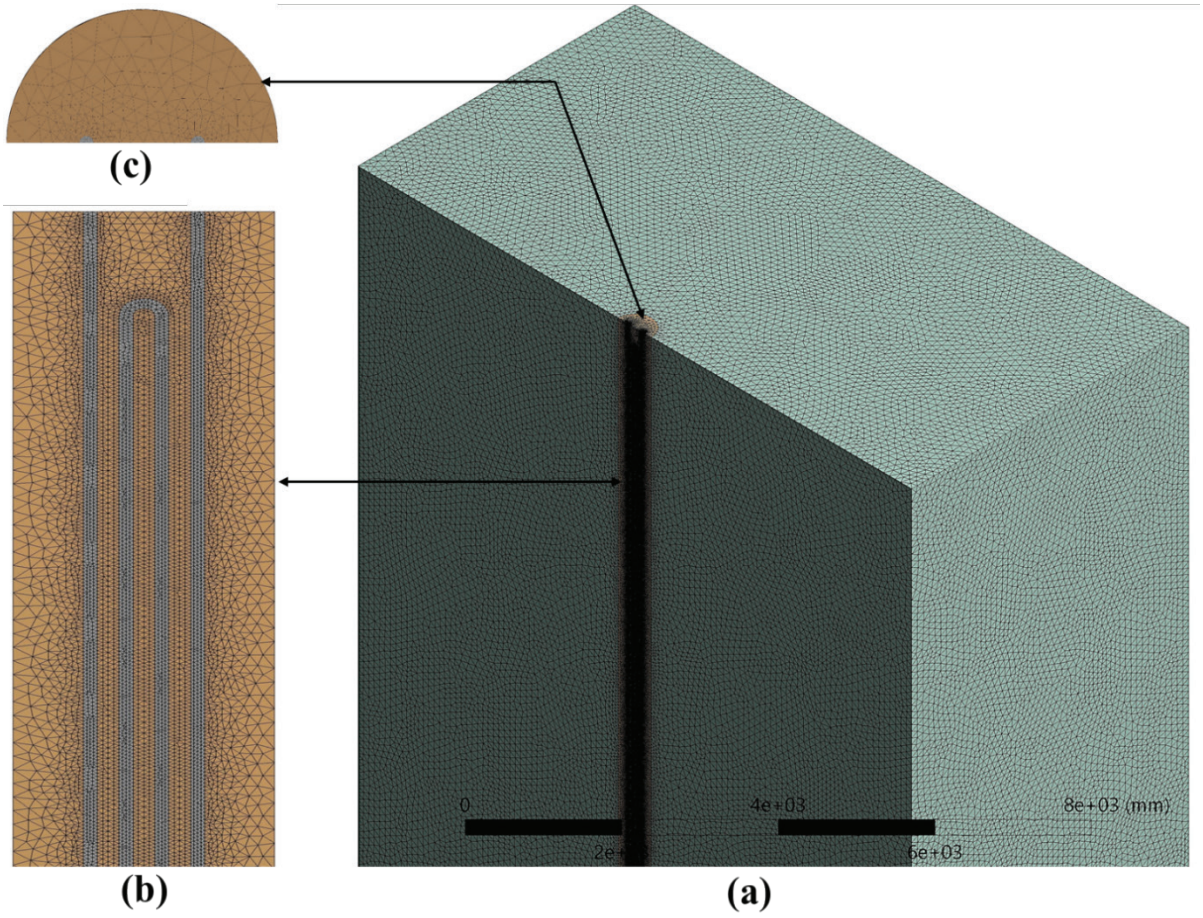

Figure 2. Illustration of mesh generation.

of the air at the outflow, which correspond to the various grid sizes, are depicted in Figure 3(a). This is being done to confirm the reliability of the results. In the figure, in element no. 23620924, the outlet air temperature came to 27.1 °C. This is selected for further calculation. Keeping all the dimensions the same and the flow inlet and boundary conditions, the model is validated, as shown in Figure 3(b). To assess the workflow, the model was validated & compared with Chen et al. [12] with an error of 1.48%. In contrast, the information about the mesh generation is listed in Table 5.

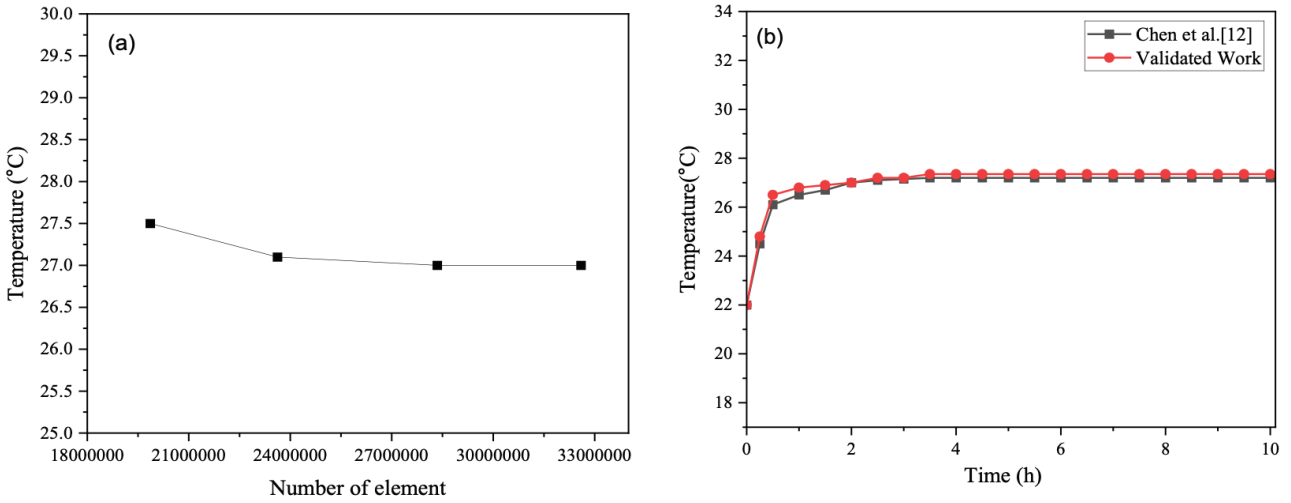

Figure 3. Illustration of (a) Mesh independency test, and (b) Model validation.

Table 5. Information about the mesh generation with mesh quality

Parameters	Value & description	Parameters	Value
Type of mesh	Tetrahedrons	Mesh quality (in avg.)	
Mesh method	Patch conforming	Aspect Ratio	1.78800
Element size	1000 mm	Skewness	0.20527
No. of elements	23620924	Orthogonal Quality	0.79354
No. of nodes	4100399	-	-

RESULTS AND DISCUSSION

In this study, numerical investigations were carried out for air velocities between 0.5 ms^{-1} and 5 ms^{-1} over 12 hours. Temperature, pressure, and velocity contours were used to improve understanding of fluid dynamics and heat transfer. Important insights are provided by these contours: Velocity contours display flow patterns, pressure contours draw attention to variations, and temperature contours display thermal gradients. To avoid repetition, only the contours for 3 ms^{-1} and 5 ms^{-1} are presented. Figures 4, 5, and 6 show the temperature, pressure, and velocity contours for these velocities. Figure 4 shows the difference in temperature between the inlet and outlet at velocity levels 3 ms^{-1} and 5 ms^{-1} respectively. Figure 4(a) shows a 9°C difference in temperature at 3 ms^{-1}, while Figure 4(b) shows a temperature difference of 7°C at 5 ms^{-1}. This signifies a decreasing temperature gradient between the inlet and outlet with increasing velocity. Figure 5 shows the pressure contour at velocity levels 3 ms^{-1} and 5 ms^{-1}. From Figures 5(a) and 5(b), it is observed that the pressure drop between the inlet and outlet at 3 ms^{-1} is around 6.26 MPa whereas at 5 ms^{-1} the pressure drop was found to be 8.91 MPa. Thus, by increasing the velocity from 3 ms^{-1} to 5 ms^{-1}, the pressure fall between the inlet and outlet increases. Finally, Figure 6 shows the velocity contour at 3 ms^{-1} and 5 ms^{-1}. The velocity of air remains constant throughout the tube.

Figure 7(a) illustrates the change in temperature at the GHE outlet with time. The simulation was conducted with different air velocities, from 0.5 ms^{-1} to 5 ms^{-1}, over a period of 12 hours of operation. For all air velocities, initially, the temperature at the outlet was low, but after some time, it gradually increased and eventually stabilized. The inlet air temperature was 309 K for all air velocities. As seen in the figure, the outlet temperature was recorded to be 299.91 K 300.03 K, 300.12 K, 300.21K, 300.38 K, 300.62 K, K, 300.9 K, 301.24 K, 301.53 K, 301.8 K for 0.5 ms^{-1} to 5 ms^{-1} correspondingly the temperature difference or drop in air temperature, shown in Fig. 7(b), was 9.09 °C, 8.97 °C, 8.88 °C, 8.79 °C, 8.62 °C, 8.38 °C, 8.1 °C, 7.76 °C, 7.47 °C, and 7.2 °C for 0.5 ms^{-1} to 5 ms^{-1} respectively. When air velocity is 5 ms^{-1}, the difference in temperature between inlet and output is lower than that of when air velocity is 0.5 ms^{-1}. Thus, upon increasing the air speed, the outlet temperature rises. Due to relatively lower velocity, the air comes in contact relatively more time through the tube with the PCM and therefore, the temperature drop may occur more than the higher velocity over time. A greater temperature drop is the result of improved cooling caused by increased air-PCM

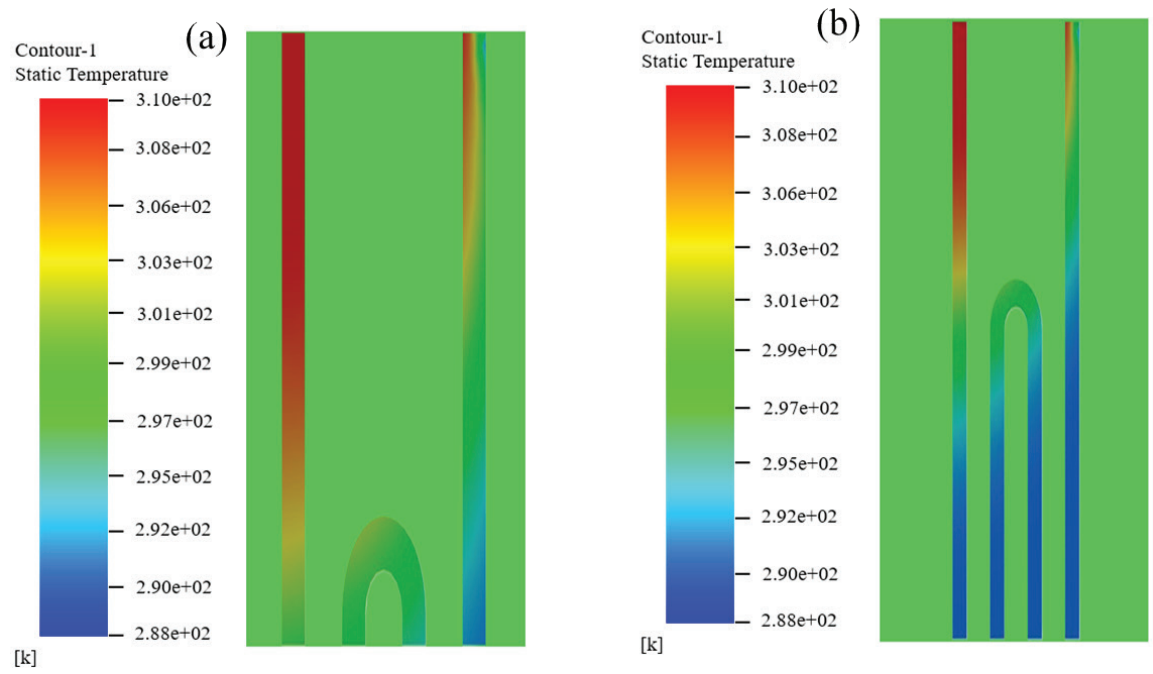

Figure 4. Temperature contour of the tube with PCM at an air velocity of (a) 3 ms^{-1} and (b) 5 ms^{-1}.

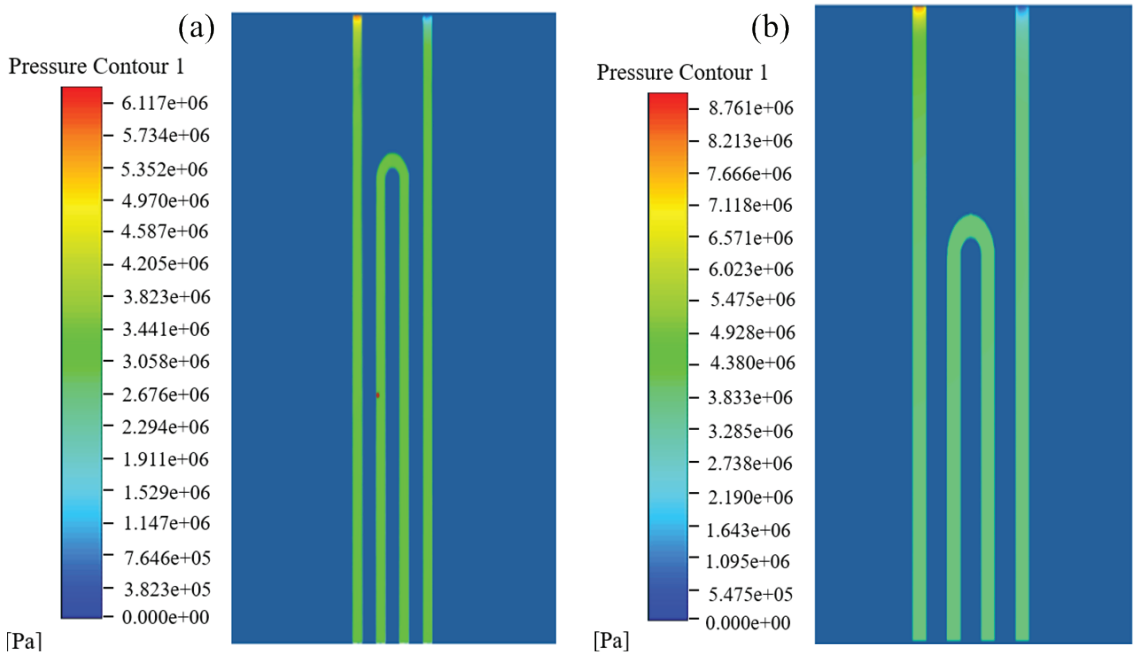

Figure 5. Pressure contour of the tube with PCM at an air velocity of (a) 3 ms^{-1} and (b) 5 ms^{-1}.

interaction. Therefore, the air velocity should be decreased from the standpoint of exit temperature.

Figure 8 depicts the heat transfer rate over time for different air velocities. Initially, a higher heat transfer rate was found for all cases; over time it decreases and eventually becomes almost constant and remains horizontal for all air velocities. First, there exists a significant difference in temperature between the soil and air before the system begins to function. When the system begins to work, the soil around the buried pipes progressively gets heated up, reducing this difference between the two as heat is being dissipated to the surrounding soil. Thus, this also reduces the reducing heat

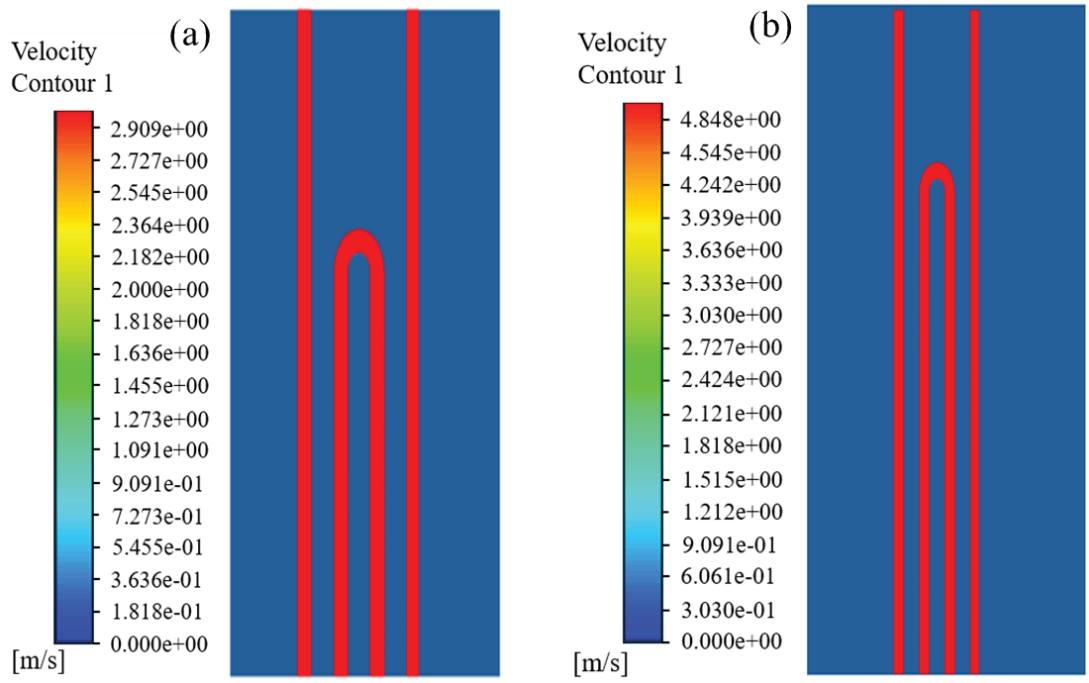

Figure 6. Velocity contour of the tube with PCM at an air velocity of (a) 3 ms^{-1} and (b) 5 ms^{-1}.

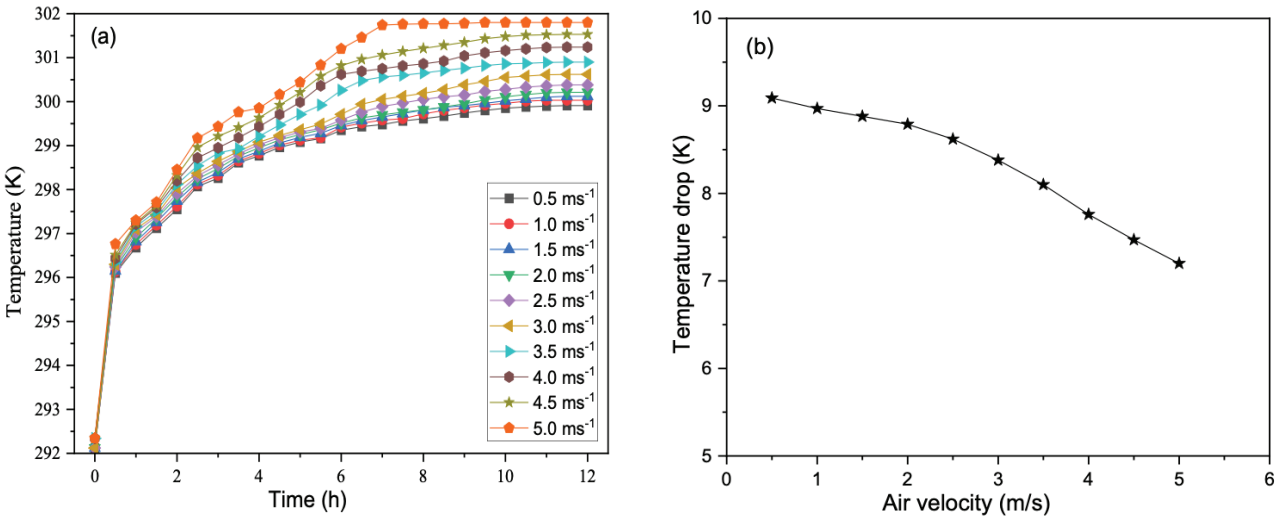

Figure 7. Illustration for the GHE: (a) temperature changes at the outlet over time and (b) variation of temperature drop with air velocities 0.5 ms^{-1} to 5 ms^{-1}.

transfer. After 12 hours of operation, the mean heat transfer rate per meter was 76.27 Wm^{-1}, 80.08 Wm^{-1}, 83.98 Wm^{-1}, 88.7 Wm^{-1}, 93.05 Wm^{-1}, 97.97 Wm^{-1}, 102.66 Wm^{-1}, 107.35 Wm^{-1}, 111.61 Wm^{-1} and 116.45 $Wm^{-1}$for air velocities from 0.5 ms^{-1} to 5 ms^{-1} respectively. It is also noticed from the figure that despite having a larger temperature drop at a lower velocity, the heat transfer rate of the system increases as air velocity increases. The rate of heat transfer per meter at 0.5 ms^{-1} is lower than that of 5 ms^{-1}. Compared to 0.5 ms^{-1} the heat transmission rate per meter for 5 ms^{-1} is roughly 65.5% higher. This is because, at higher air velocity, the boundary layer is comparatively thinner, which results in the convective heat transfer coefficient increasing, which ultimately contributes to the increased heat transfer. Secondly, a higher velocity of air means higher turbulence, which results in better air mixing, this also accelerates the heat transfer rate. A higher air velocity is therefore preferred in terms of when a better heat transfer rate per meter is desired.

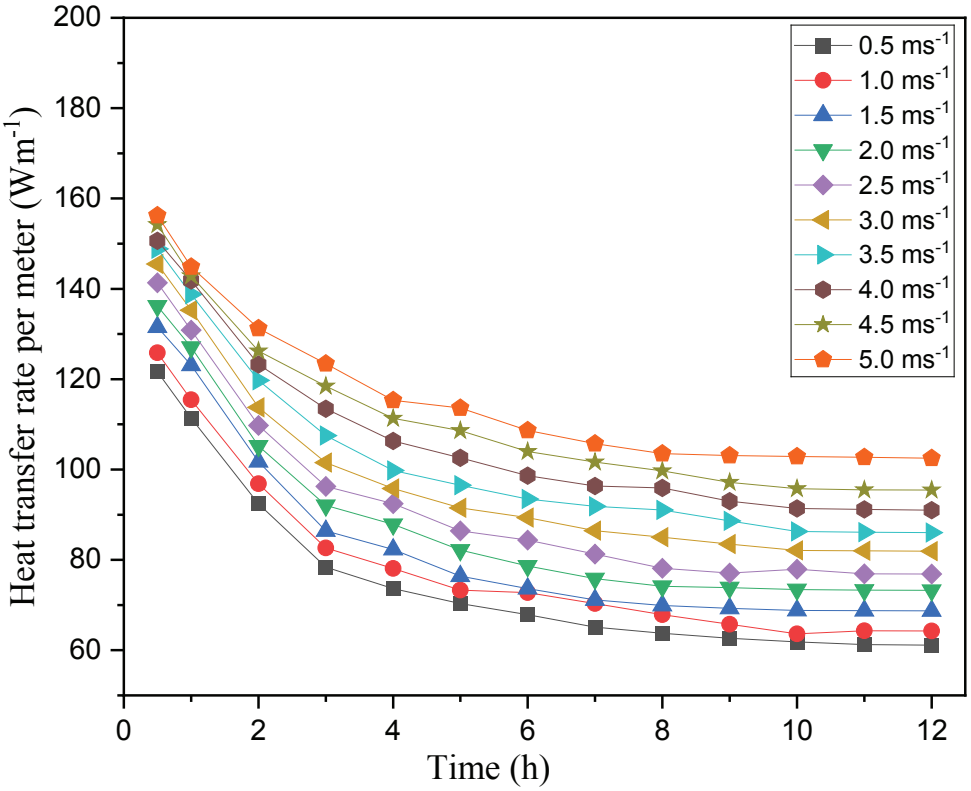

Figure 8. Heat transfer rates per meter over time for different air velocities.

Figure 9 depicts variation in cooling capacity with time at different air velocities. Initially, a large temperature gradient between hot air and the ground is responsible for the heat transfer, and as the warm air circulates through the system, it gradually cools down. During the first half of the system's operation, cooling capacity increases because air gives up its heat to the ground, with higher air velocities resulting in faster circulation and more heat transfer. The cooling capacity continues to rise further and reaches its maximum point around 6 hours in all velocity levels, with the maximum values being: 1,297.01 W at 5.0 ms^{-1}, 1,243.28 W at 4.5 ms^{-1}, 1,180.6 W at 4.0 ms^{-1}, 1,120.15 W at 3.5 ms^{-1}, 1,064.18 W at 3.0 ms^{-1}, 1,017.16 W at 2.5 ms^{-1}, 999.254 W at 2.0 ms^{-1}, 976.866 W at 1.5 ms^{-1}, 941.045 W at 1.0 ms^{-1}, and 925.373 W at 0.5 ms^{-1}. Upon reaching the maximum point in each case, the temperature differential between air and ground is at its most efficient for heat transfer as the air has cooled as much as it can. However, there is a decline in cooling capacity afterward. This is due to the temperature differential responsible for heat transfer decreases as air temperature gradually approaches the ground temperature.

Figure 10 illustrates the effectiveness of the GHE system over the period of operation time. The effectiveness of the GHE system during each hour of a 12-hour operation has been calculated from Eq. (11). After an hour of continuous operation, the system's maximum effectiveness was found to be between 64% and 61% for all air velocities. The effectiveness decreases in a similar trend for all velocities over the period of system functioning. Consequently, the effectiveness was determined to be 47%, 44%, 46.5%, 46%, 45%, 44%, 42%, 40%, 39%, and 37% for 0.5 ms^{-1} to 5 ms^{-1}, respectively, at 12 hours of continuous operation. According to the results, the ground heat exchanger (GHE) system's effectiveness steadily declines during operation. After 12 hours of continuous operation, effectiveness drops by about 26.56% for 0.5 ms^{-1} and 39.34% for 5 ms^{-1} than that after 1 hour of operation. Hence, the GAHE system is found to be more effective at 0.5 ms^{-1} than at 5 ms^{-1}. Effectiveness reduces over time primarily because of the diminishing temperature gradient between the ground and the incoming air. As the air passes through the GHE, it gradually warms up, reducing the driving force for heat transfer. Higher air velocities, although they increase the heat transfer rate, result in a smaller temperature gradient between air and ground, leading to lower effectiveness. Conversely, lower velocities maintain a higher temperature difference for a longer period, which helps sustain the system's effectiveness over time.

Figure 11 illustrates the air temperature variation along the length of the pipe in the ground heat exchanger after 12 hours of uninterrupted operation, which is essential for accurately ascertaining the required pipe length. The length of the pipe is one of the prime factors that control the cost associated with the construction of GHE. Consequently,

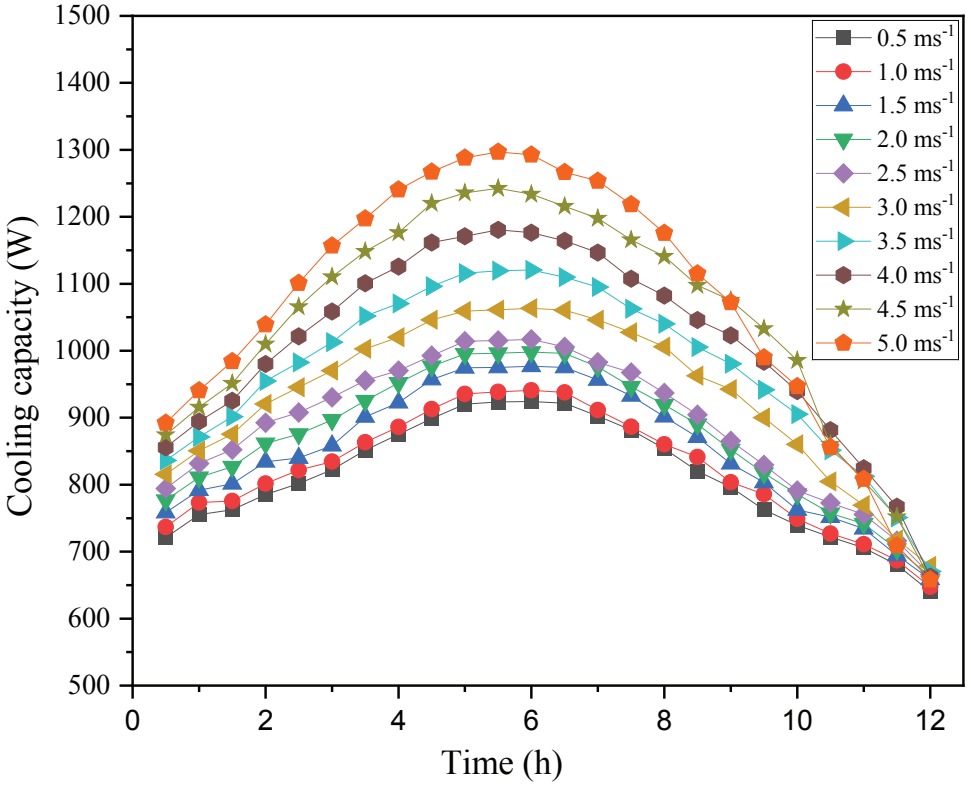

Figure 9. Cooling capacity variation with time as a function of air speed.

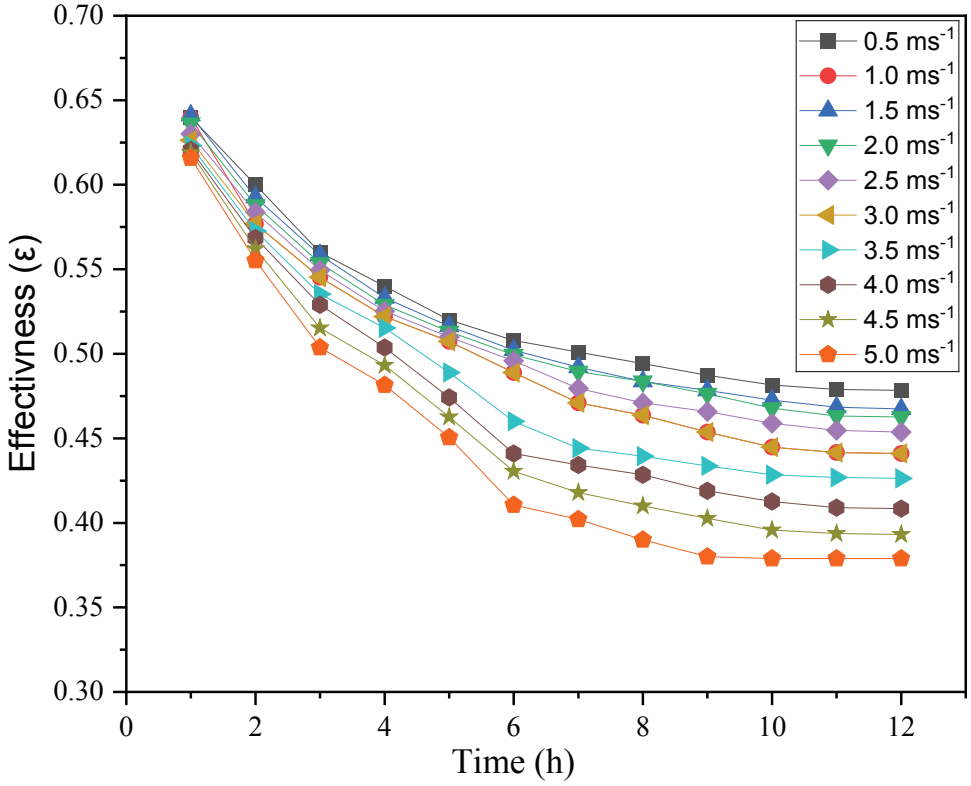

Figure 10. Effectiveness of ground heat exchanger (GHE) system.

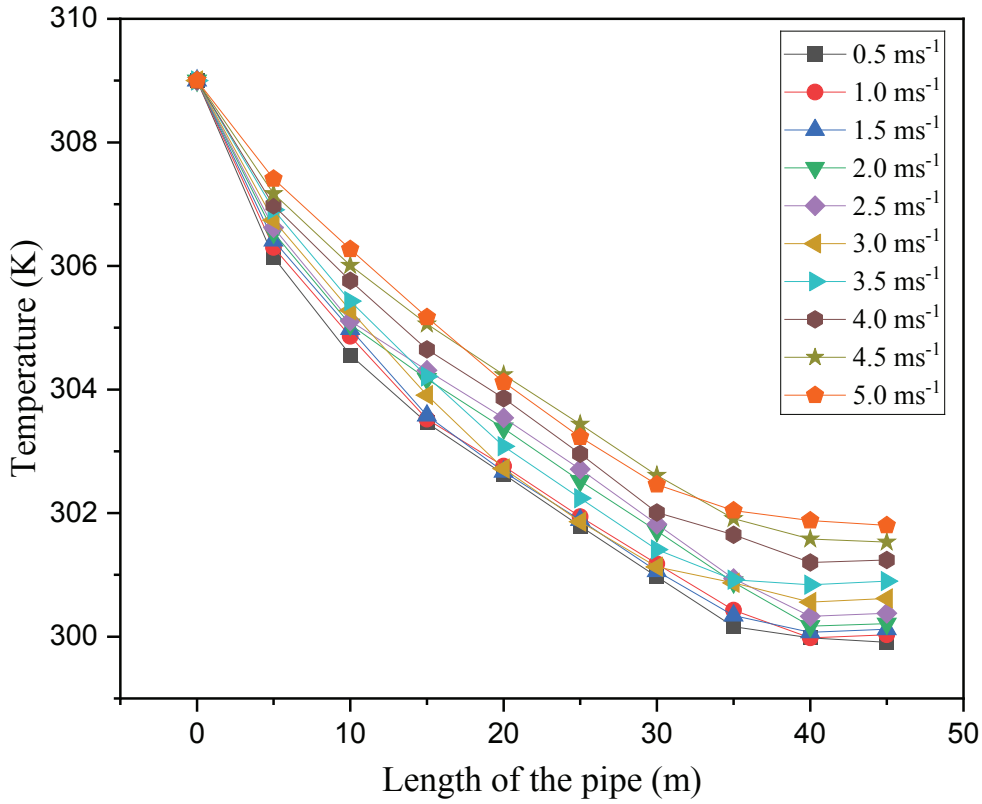

Figure 11. Variation of air temperature along the pipe length after 12 h of continuous operation.

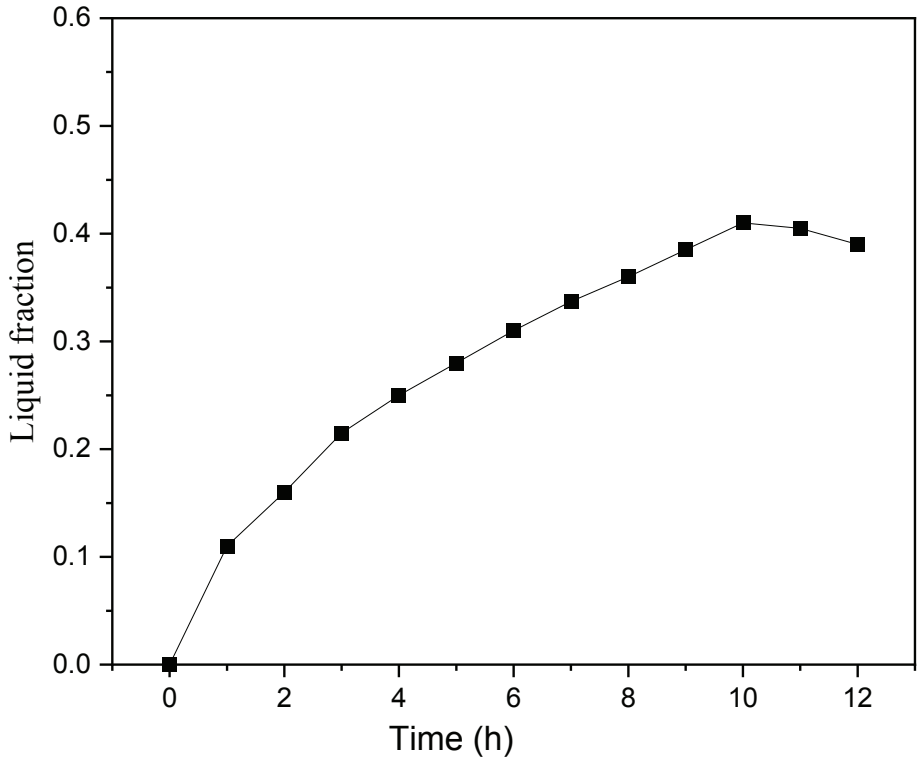

Figure 12. Variation of the liquid fraction of PCM with time.

while designing the system, it is essential to compute the necessary length for a specific reduction in air temperature. The length of the pipe is dictated by the thermophysical properties of the adjacent soil. At 12 hours of uninterrupted operation, a decrease in temperature of 9.09 °C is observed at the outlet of the ground heat exchanger with a flow rate of 0.5 ms^{-1}. After 40 meters, the graph became steady, and beyond that distance, the temperature decrease was minimal.

Figure 12 illustrates the progression of the liquid fraction of the phase change material (PCM) with time of operation. The liquid percentage of PCM initially increases over time, then declines after attaining its maximum value. The solid PCM process begins with the 0% liquid fraction. Upon receiving heat, the temperature of the PCM starts to increase, eventually reaching the melting point, and then the liquid fraction starts to rise. At the melting point, the temperature remains constant, and solids and liquids coexist. The liquid fraction approaches 100%, indicating the conclusion of the melting phase. When heat is withdrawn, the liquid fraction declines, but initially remains at 100% until solidification. The explanation is that the ambient air temperature exceeds and falls below the phase change temperature (PCT) during the charging and discharging phases, respectively.

In Figures 13 and 14, the heat transfer characteristics (Nusselt number and heat transfer coefficient) were plotted against Reynolds number, and all the data showed an increasing trend with the increase in Reynolds number. The heat transfer characteristics, including the average Nusselt number and average heat transfer coefficient, increased with the rise in the Reynolds number, which indicated more turbulent flow. Turbulence enhanced fluid mixing and thinner the thermal boundary layer around the pipe, which causes more effective convective heat transfer. It is noted that higher air velocity has a higher heat transfer coefficient.

Figure 15 illustrates the disparity in output temperature between the GHE utilizing phase change material and a conventional GHE. The GHE utilizing phase change material exhibits a lower exit temperature compared to the alternative. Phase change material absorbs heat from the surroundings with its large latent heat. So, the heat exchanger's performance is improved by using phase change material. Conventional GHEs are reliable and effective for heating and cooling, but their performance can be affected by seasonal variations and thermal depletion. GHEs with PCMs allow the system to store excess thermal energy when temperatures are high, for later use, ensuring better thermal regulation. It offers improved efficiency by stabilizing temperatures within the system. The PCM's ability to absorb and release heat helps mitigate temperature fluctuations, leading to better performance in peak load situations.

Figure 16 depicts the comparison between the results of the study conducted by Mathur et al. [55], Zhou et al. [33], Yusof et al. [18], Yang et al. [16], Agrawal et al. [60] and

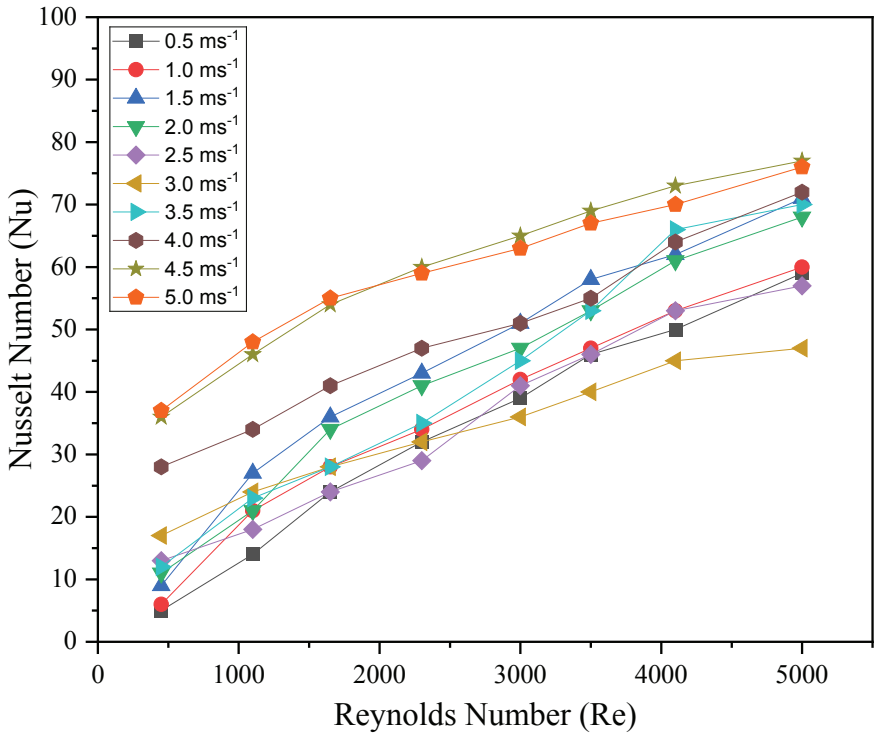

Figure 13. Nusselt number variation with Reynolds number at different air velocity.

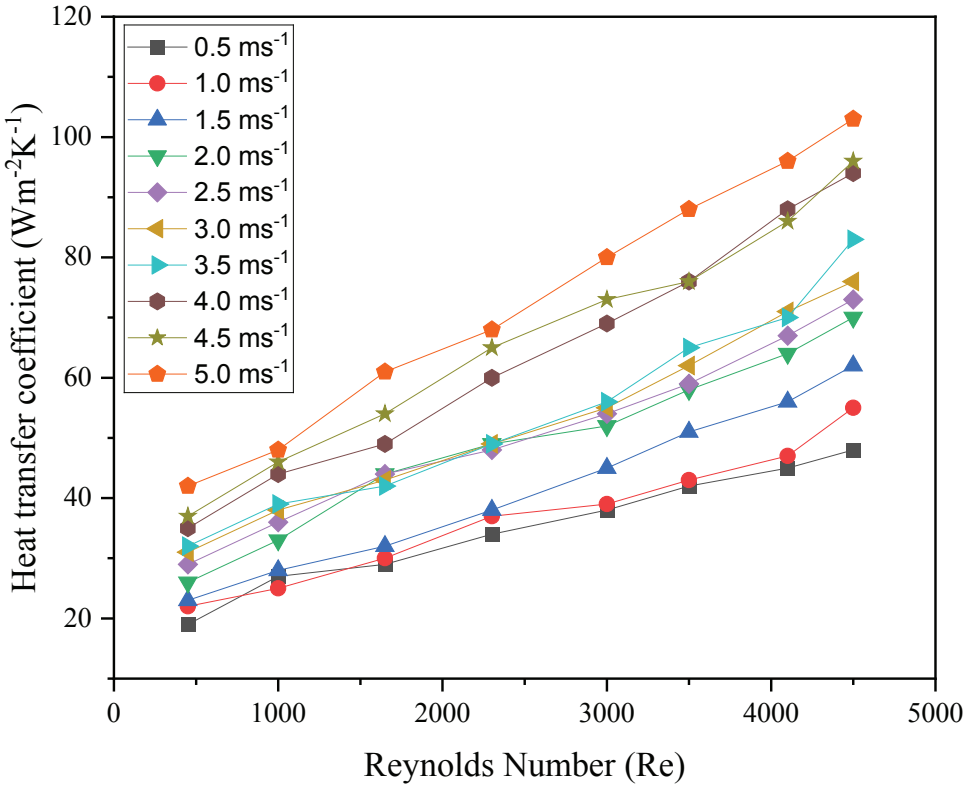

Figure 14. Various heat transfer coefficients with Reynolds number for different air velocities.

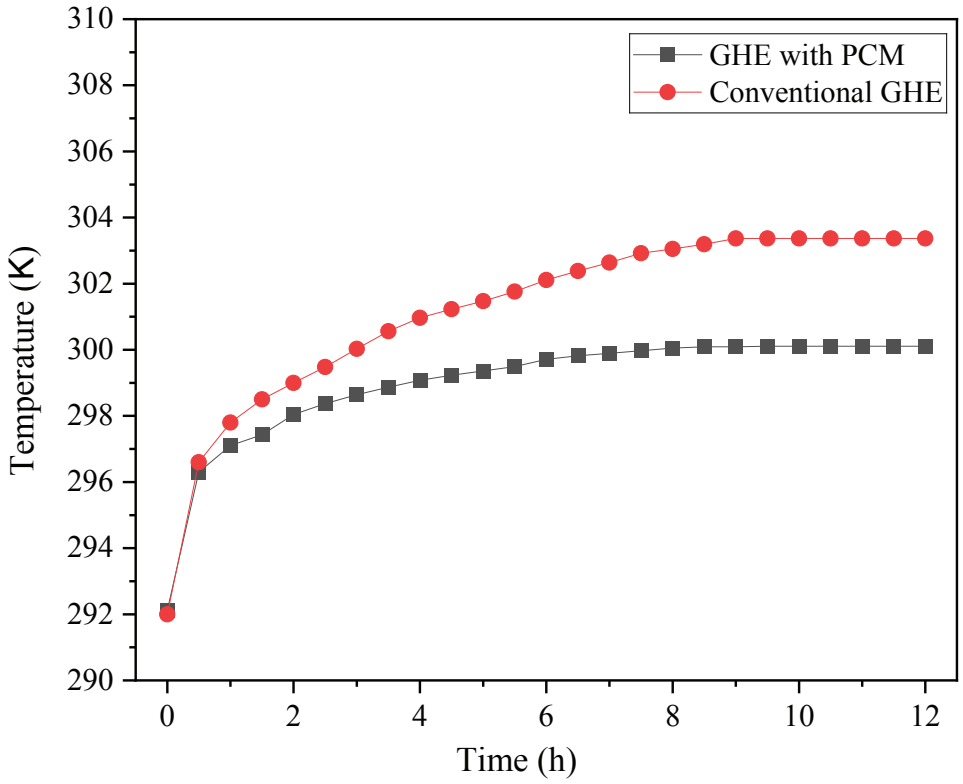

Figure 15. Comparison of GHE with PCM against conventional GHE at a velocity of 5 ms^{-1}.

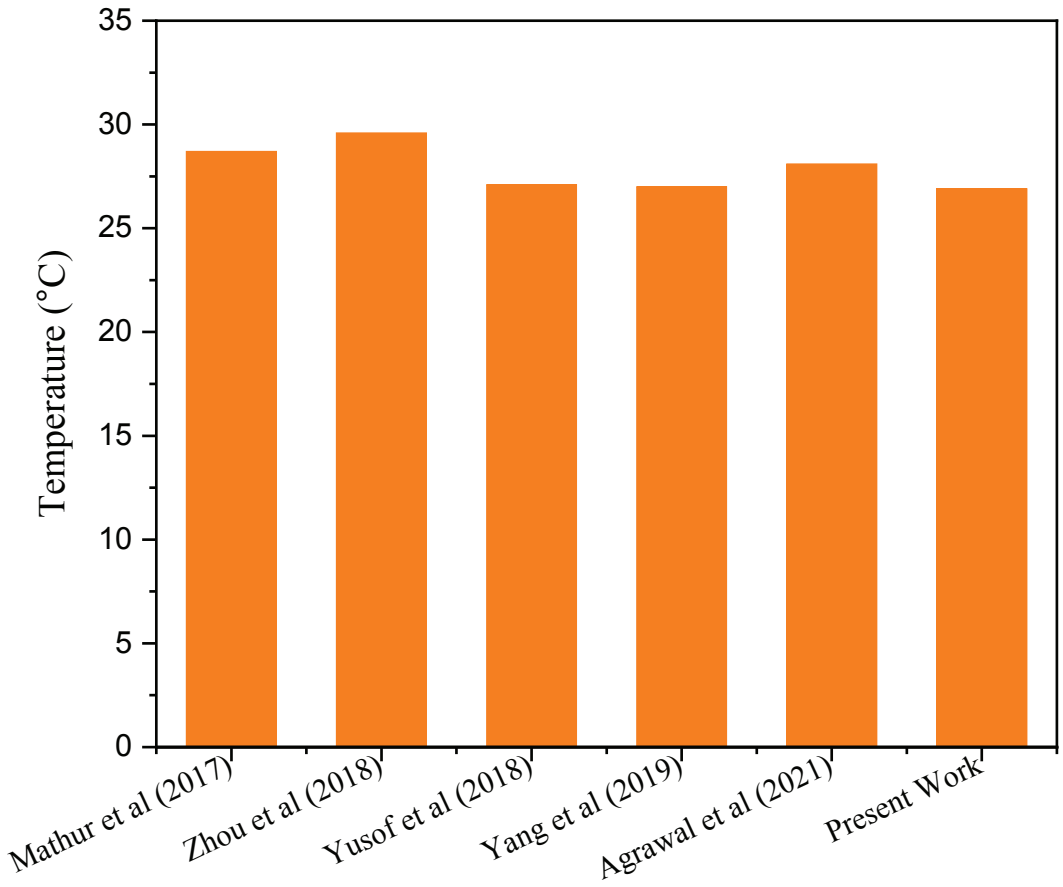

Figure 16. Comparison of the temperature variation of this work over previous studies on GSHE.

the present study. In these studies, the outlet temperature of GHE is found to be 28.7 °C, 29.6 °C, 27.1 °C, 27 °C, 28.1 °C, and 26.9 °C. Thus, compared to previous studies, the lowest ground temperature of the heat pump was observed in the present study. Where Figure 17 compares the effectiveness of the GHE across studies conducted by Zhang et al. [64], Hu et al. [65], Chen et al. [13], and the present study. After 10 hours of operation, the effectiveness values were 0.07821, 0.2475, 0.179191, and 0.48158, 0.46789, 0.37895, respectively, depending on the conditions used. Zhang et al. used a horizontal tube setup at 2 ms^{-1}, while the present study used a vertical arrangement, showing a much higher effectiveness of 0.46789—about six times greater than Zhang et al.'s result. Hu et al.'s effectiveness, measured at a lower velocity of 0.419 ms^{-1}, was still lower than even the minimum value of effectiveness from the present study at 5 ms^{-1}. As for Chen et al., who also used paraffin wax as the PCM, their results were 0.472 times lower than the lowest effectiveness observed in the present study, even at a velocity of 0.3 ms^{-1}. These differences can be explained by variations in the dimensional parameters and operating conditions between the studies.

Meanwhile, Figure 18 shows the heat transfer rate per meter across studies conducted by Jalaluddin and Miyara [66], who used water as the working fluid at a flow rate of 4 l/min and silica sand as the backfill material, Kim et al. [67], using the same working fluid at a speed of 0.3 ms^{-1} with cement-based grouts, Yang et al. [16], also used water at 0.6 ms^{-1} with oleic acid as the backfill material and the present study where PCM was used as the backfill material with air as the working fluid and in this case, at a velocity of 0.5 ms^{-1}. Although the operational parameters such as velocity, soil temperature, and U-Tube dimensions differ in each case, due to the variation in these parameters, the thermal performance of the GHE may vary and differ from one study to another. The comparison aims to showcase how the Ground Source Heat Exchanger (GHE) responds to various backfill materials. After 12 hours of operation, the PCM-coupled GHE of the present study achieves a heat transfer rate of 61.12 W/m, which is 2.27 times higher than the result obtained by Jalaluddin and Miyara [66] and 1.05 times greater than that of Kim et al. [67]. The present study also shows a heat transfer rate 2.5 times greater than that of Yang et al. [16] after 10 hours of operation. Thus, the GHE with PCM as the backfill material and air as the working fluid demonstrates a better heat transfer rate per meter than the other three studies.

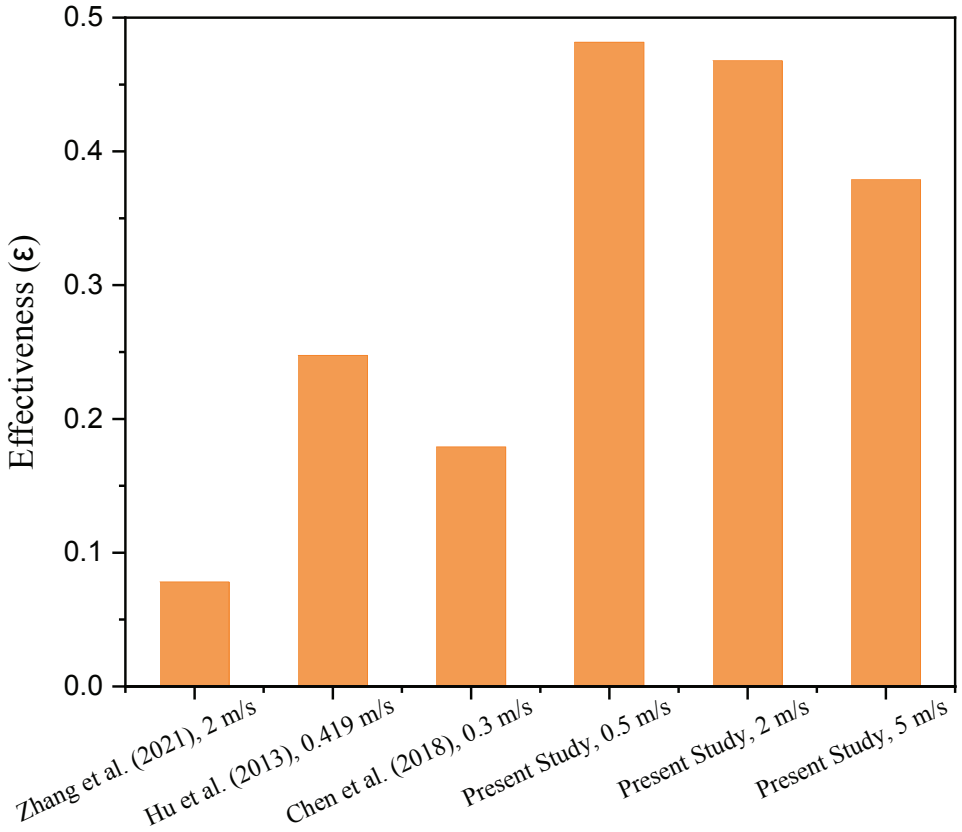

Figure 17. Effectiveness variation of the work compared to the previous studies on GSHE.

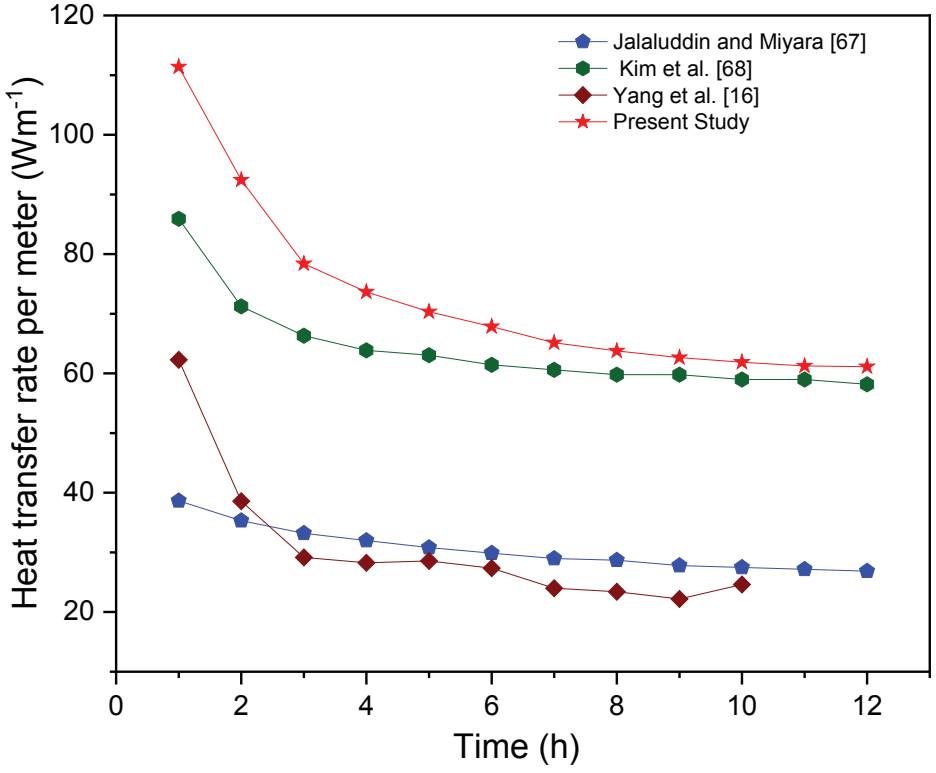

Figure 18. Variation of the heat transfer rate per meter of the present study compared with previous studies on GSHE.

CONCLUSION

In this study, the main concentration was on the thermal performance of an underground u-bend type heat exchanger with phase change material. A double U-shape tube was designed and numerically simulated under certain conditions. In this work, paraffin wax was used as PCM in the backfilling of the borehole around the pipe. Outlet temperature, rate of heat transfer, cooling capacity, and effectiveness of the system were measured and plotted in the graph and compared for air velocity ranging from 0.5 ms^{-1} to 5 ms^{-1}. In summary, the subsequent findings have been discovered.

- A reduced air velocity should result in a lower heat exchanger exit temperature. The temperature drop at the exit was 9.09°C and 7.2°C respectively for air velocity 0.5 ms^{-1} and 5 ms^{-1} after 12 hours of continuous operation. Therefore, the finding recommends a lower velocity flow for a better temperature drop at the outlet
- At higher speeds, the heat transfer rate increases. The heat transfer rate per meter is 76.27 Wm^{-1} for 0.5 ms^{-1} and 116.45 Wm^{-1} for 5 ms^{-1} air velocity after 12 hours of operation. Therefore, to obtain a high heat transfer rate per meter, high air velocity is preferred. This is true for the overall cooling capacity as well.
- The system's effectiveness declines with time. The parameter decreases by 26.56% and 39.34% for 0.5 ms^{-1} and 5 ms^{-1}, respectively, after 12 hours of uninterrupted operation in comparison to the outcomes after 1 hour of operation. Additionally, the system's effectiveness during any given operating hour was shown to decline as air velocity increased.
- After 40 m length of the GHE, the change in temperature is minimal.
- Thus, high air velocity is preferable for higher heat transfer rate and cooling capacity, but higher velocity increases the outlet temperature and results in reduced temperature drop between inlet and outlet and decreased effectiveness.

The study reveals that using PCM as the backfill with good thermal qualities near ground heat exchanger pipes enhances the overall performance of the system. Additionally, the ground heat exchanger's length may be significantly reduced by using U-tubes. Ground heat exchangers are energy-efficient, adaptable heating and cooling systems used in both commercial and residential establishments. They work in every climatic condition and can cut carbon emissions. Future studies should concentrate on enhancing system performance under a variety of environmental circumstances, design optimization which also includes finding the optimal length of the GHE, and thermal performance enhancement with phase change materials.

NOMENCLATURE

A_{Mush}	Mushy zone constant
CE	Convective heat flow between the soil surface and ambient air, (W/m^2)
$EAHE$	Earth air heat exchanger
GHE	Ground heat exchanger
$GSHP$	Ground source heat pump
G	Incident solar global irradiance, (W/m^2)
$HVAC$	Heating, ventilation, and air conditioning
HTF	Heat transfer fluid
$HEPC$	Horizontal earth pipe cooling
$HWAHE$	Helical water air heat exchanger
ΔH	Latent enthalpy, (J/kg)
LR	Soil surface emitted long-wave radiation, (W/m^2)
$SSPCM$	Shape stabilized phase change material
T_{soil}	Soil natural temperature field, (°C)
$T_{sol\text{-}air}$	Solar-air temperature, (°C)
T_{ss}	Source term energy, W/m^3
T_{amb}	Ambient air temperature, (°C)
$T_{amb,m}$	Mean of monthly ambient air temperature, (°C)

AUTHORSHIP CONTRIBUTIONS

Md. Nur Alam (M. N. Alam): Conceptualization, methodology, investigation, data acquisition, analysis, writing original draft, and editing manuscript.

Dipayan Mondal (D. Mondal): Conceptualization, methodology, investigation, analyzing and interpreting the data, writing, review and editing, writing of reviewer response, discussion, and supervising.

Mohammad Rafat Islam (M. R. Islam): Analyzing and interpreting the data, reviewing and editing, and writing reviewer response.

DATA AVAILABILITY STATEMENT

The corresponding author will make the data available upon reasonable request.

CONFLICT OF INTEREST

There were no conflicts of interest disclosed by the authors, nor was there any major financial contribution that could have impacted on the outcome of this study

ETHICS

The publication of this manuscript raises no ethical issues.

STATEMENT ON THE USE OF ARTIFICIAL INTELLIGENCE

Artificial intelligence was not used in the preparation of the article.

REFERENCES

[1] Omer AM. Energy, environment and sustainable development. Renew Sustain Energy Rev 2008;12:2265– 2300. [CrossRef]

[2] Sawhney RL, Buddhi D, Thanu NM. An experimental study of summer performance of a recirculation type underground airpipe air conditioning system. Build Environ 1998;34:189–196. [CrossRef]
[3] Esen M, Yuksel T. Experimental evaluation of using various renewable energy sources for heating a greenhouse. Energy Build 2013;65:340–351. [CrossRef]
[4] Naili N, Hazami M, Kooli S, Farhat A. Energy and exergy analysis of horizontal ground heat exchanger for hot climatic condition of northern Tunisia. Geothermics 2015;53:270–280. [CrossRef]
[5] Santamouris M, Mihalakakou G, Balaras CA, Lewis JO, Vallindras M, Argiriou A. Energy conservation in greenhouses with buried pipes. Energy 1996;21:353–360. [CrossRef]
[6] Mihalakakou G, Lewis JO, Santamouris M. On the heating potential of buried pipes techniques — application in Ireland. Energy Build 1996;24:19–25. [CrossRef]
[7] Kong XR, Deng Y, Li L, Gong WS, Cao SJ. Experimental and numerical study on the thermal performance of ground source heat pump with a set of designed buried pipes. Appl Therm Eng 2017;114:110–117. [CrossRef]
[8] Pu L, Qi D, Li K, Tan H, Li Y. Simulation study on the thermal performance of vertical U-tube heat exchangers for ground source heat pump system. Appl Therm Eng 2015;79:202–213. [CrossRef]
[9] Jalaluddin, Miyara A, Tsubaki K, Inoue S, Yoshida K. Experimental study of several types of ground heat exchanger using a steel pile foundation. Renew Energy 2011;36:764–771. [CrossRef]
[10] Liu Q, Huang Y, Ma Y, Peng Y, Wang Y. Parametric study on the thermal performance of phase change material-assisted earth-to-air heat exchanger. Energy Build 2021;238. [CrossRef]
[11] Gao J, Zhang X, Liu J, Li KS, Yang J. Thermal performance and ground temperature of vertical pile-foundation heat exchangers: A case study. Appl Therm Eng 2008;28;2295–2304. [CrossRef]
[12] Chen F, Mao J, Li C, Hou P, Li Y, Xing Z, et al. Restoration performance and operation characteristics of a vertical U-tube ground source heat pump system with phase change grouts under different running modes. Appl Therm Eng 2018;141:467–482. [CrossRef]
[13] Chen F, Mao J, Chen S, Li C, Hou P, Liao L. Efficiency analysis of utilizing phase change materials as grout for a vertical U-tube heat exchanger coupled ground source heat pump system. Appl Therm Eng 2018;130:698–709. [CrossRef]
[14] Qi D, Pu L, Sun F, Li Y. Numerical investigation on thermal performance of ground heat exchangers using phase change materials as grout for ground source heat pump system. Appl Therm Eng 2016;106:1023–1032. [CrossRef]
[15] Ahmed SF, Amanullah MTO, Khan MMK, Rasul MG, Hassan NMS. Parametric study on thermal performance of horizontal earth pipe cooling system in summer. Energy Convers Manag 2016;114:324–337. [CrossRef]
[16] Yang W, Xu R, Yang B, Yang J. Experimental and numerical investigations on the thermal performance of a borehole ground heat exchanger with PCM backfill. Energy 2019;174:216–235. [CrossRef]
[17] Bottarelli M, Bortoloni M, Su Y, Yousif C, Aydin AA, Georgiev A. Numerical analysis of a novel ground heat exchanger coupled with phase change materials. Appl Therm Eng 2015;88:369–375. [CrossRef]
[18] Yusof TM, Ibrahim H, Azmi WH, Rejab MRM. Thermal analysis of earth-to-air heat exchanger using laboratory simulator. Appl Therm Eng 2018;134:130–140. [CrossRef]
[19] Li C, Mao J, Zhang H, Xing Z, Li Y, Zhou J. Numerical simulation of horizontal spiral-coil ground source heat pump system : Sensitivity analysis and operation characteristics. Appl Therm Eng 2017;110:424–435. [CrossRef]
[20] Misra R, Bansal V, Agrawal GD, Mathur J, Aseri TK. CFD analysis based parametric study of derating factor for Earth Air Tunnel Heat Exchanger. Appl Energy 2013;103:266–277. [CrossRef]
[21] Florides G, Theofanous E, Joseph-Stylianou J, Tassou S, Christodoulides P, Zomeni Z, et al. Vertical and Horizontal Ground Heat Exchanger Modeling. In Proceedings of the Conference: World Renewable Energy Congress, 2013, KTISIS Institutional Repository, Cyprus University of Technology, Cyprus.
[22] Cui Q, Shi Y, Zhang Y, Wu R, Jiao Y. Comparative study on the thermal performance and economic efficiency of vertical and horizontal ground heat exchangers. Adv Geo-Energy Res 2023;7:7–19. [CrossRef]
[23] Ghosal MK, Tiwari GN. Modeling and parametric studies for thermal performance of an earth to air heat exchanger integrated with a greenhouse. Energy Convers Manag 2006;47:1779–1798. [CrossRef]
[24] Morshed W, Leso L, Conti L, Rossi G, Simonini S, Barbari M. Cooling performance of earth-to-air heat exchangers applied to a poultry barn in semi-desert areas of south Iraq. Int J Agric Biol Eng 2018;11:47–53. [CrossRef]
[25] Hsu CY, Chiang YC, Chien ZJ, Chen SL. Investigation on performance of building-integrated earth-air heat exchanger. Energy Build 2018;169:444–452. [CrossRef]
[26] Aditya GR, Mikhaylova O, Narsilio GA, Johnston IW. Comparative costs of ground source heat pump systems against other forms of heating and cooling for different climatic conditions. Sustain Energy Technol Assessments 2020;42:100824. [CrossRef]

[27] Gao B, Zhu X, Yang X, Yuan Y, Yu N, Ni J. Operation performance test and energy efficiency analysis of ground-source heat pump systems. J Build Eng 2021;41:102446. [CrossRef]
[28] Zhou Z, Liu Q, Tao Y, Peng Y, Zhou T, Wang Y. Analysis of a borehole ground heat exchanger with shape-stabilized phase change material backfill. Appl Therm Eng 2022;222. [CrossRef]
[29] Zhang XY, Ge YT, Burra, Lang PY. Experimental investigation and CFD modelling analysis of finned-tube PCM heat exchanger for space heating. Appl Therm Eng 2024;244. [CrossRef]
[30] Emmi G, Bottarelli M. Enhancement of shallow ground heat exchanger with phase change material. Renew Energy 2022;206. [CrossRef]
[31] Hadjadj A, Benhaoua B, Atia A, Khechekhouche A, Lebbihiat N, Rouag A. Air velocity effect on the performance of geothermal helicoidally water-air heat exchanger under El Oued climate, Algeria. Therm Sci Eng Prog 2019;20. [CrossRef]
[32] Han J, Cui M, Chen J, Lv W. Analysis of thermal performance and economy of ground source heat pump system: a case study of the large building. Geothermics 2021;89:101929. [CrossRef]
[33] Zhou T, Xiao Y, Liu Y, Lin J, Huang H. Research on cooling performance of phase change material-filled earth-air heat exchanger. Energy Convers Manag 2018;177:210–223. [CrossRef]
[34] Mondal D, Ikram MO, Rabbi MF, Moral MNA. Experimental Investigation and Comparison of Bend Tube Parallel & Counter Flow and Cross Flow Water to Air Heat Exchanger. Int J Sci Eng Res 2014;5:686–695.
[35] Mondal D, Alam A, Islam MA. Experimental Observation of a Small Capacity Vapor Absorption Cooling System 2014;5:456–467.
[36] Mondal D, Islam MA. Experimental Investigation on an Intermittent Ammonia Absorption Refrigeration. Mech Eng Res J 2018;11:59–65.
[37] Mondal D, Hori Y, Kariya K, Miyara A, Alam MJ. Measurement of Viscosity of a Binary Mixture of R1123 + R32 Refrigerant by Tandem Capillary Tube Method. Int J Thermophys 2020;41:1–20. [CrossRef]
[38] Mondal D, Kariya K, Tuhin AR, Amakusa N, Miyara A. Viscosity measurement for trans-1,1,1,4,4,4-hexafluoro-2-butene(R1336mzz(E)) in liquid and vapor phases. Int J Refrig 2021;133:267–275. [CrossRef]
[39] Mondal D, Kariya K, Tuhin AR, Miyoshi K, Miyara A. Thermal conductivity measurement and correlation at saturation condition of HFO refrigerant trans-1,1,1,4,4,4-hexafluoro-2-butene (R1336mzz(E)). Int J Refrig 2021;129:109–117. [CrossRef]
[40] Mondal D, Tuhin AR, Kariya K, Miyara A. Measurement of Kinematic Viscosity and Thermal Conductivity of 3,3,4,4,5,5-HFCPE in Liquid and Vapor Phases. Int J Refrig 2022;140:150–165. [CrossRef]
[41] Islam L, Mondal D, Islam A, Das P. Effects of Heat Transfer Characteristics of R32 and R1234yf with Al2O3 Nanoparticle through U-Bend Tube Evaporator. J Eng 2024:24. [CrossRef]
[42] Das P, Mondal D, Islam A, Afroj M. Thermodynamic performance evaluation of a solar powered Organic Rankine cycle (ORC) and dual cascading vapor compression cycle (DCVCC): Power generation and cooling effect. Energy Convers Manag X 2024;23:100662. [CrossRef]
[43] Arefin MM, Mondal D, Islam MA. Optimizing cascade refrigeration systems with low GWP refrigerants for Low-Temperature Applications: A thermodynamic analysis. Energy Convers Manag X 2024;24:100722. [CrossRef]
[44] Bari MA, Mondal D, Hasib MA. Impact of air flow, temperature distribution, and heat transmission in a refrigerator compartment with and without shelves: A numerical approach. J Therm Eng 2024;10:1590–1606. [CrossRef]
[45] Shaharier MT, Mondal D, Hasib MA, Islam MA. Effects of gas-liquid flow and dehumidification performance of a liquid desiccant dehumidifier: A numerical approach for vertical smooth & rough, and inclined rough plates. J Therm Eng 2024;10:1559–1576. [CrossRef]
[46] Rifert VG, Gorin VV, Sereda VV, Treputnev VV. Improving Methods to Calculate Heat Transfer During the Condensation Inside Tubes. J Eng Phys Thermophys 2019;92:797–804. [CrossRef]
[47] Rifert V, Sereda V, Gorin V, Barabash P, Solomakha A. Heat transfer during film condensation inside plain tubes. Review of experimental research. Heat Mass Transf 2020;56:691–713. [CrossRef]
[48] Thome JR, Hajal J, Cavallini A. Condensation in horizontal tubes, part 2: New heat transfer model based on flow regimes. Int J Heat Mass Transf 2003;46:3365–3387. [CrossRef]
[49] Cavallini A, Col DD, Doretti L, Matkovic M, Rossetto L, Zilio C, et al. Condensation in horizontal smooth tubes: A new heat transfer model for heat exchanger design. Heat Transf Eng 2006;27:31–38. [CrossRef]
[50] Shah MM. A new flow pattern based general correlation for heat transfer during condensation in horizontal tubes. IHTC 2014;1–15. [CrossRef]
[51] Rifert VG, Sereda VV, Barabash PO, Gorin VV. Condensation inside smooth horizontal tubes: Part 2. improvement of heat exchange prediction. Therm Sci 2017;21:1479–1489. [CrossRef]
[52] Rifert V, Sereda V, Gorin V, Barabash P, Solomakha A. Substantiation and the range of application of a new method for heat transfer prediction in condensing inside plain tubes. Energetika 2018;64:146–154. [CrossRef]

[53] Camaraza-Medina Y, Hernandez-Guerrero A, Luviano-Ortiz JL, Mortensen-Carlson K, Cruz-Fonticiella OM, García-Morales OF. New model for heat transfer calculation during film condensation inside pipes. Int J Heat Mass Transf 2019;128:344–353. [CrossRef]

[54] ANSYS. ANSYS Fluent Theory Guide. Available at: https://dl.cfdexperts.net/cfd_resources/Ansys_Documentation/Fluent/Ansys_Fluent_Theory_Guide.pdf. Accessed on 28 Feb 2026.

[55] Mathur A, Priyam, Mathur S, Agrawal GD, Mathur J. Comparative study of straight and spiral earth air tunnel heat exchanger system operated in cooling and heating modes. Renew Energy 2017;108:474–487. [CrossRef]

[56] Tay NHS, Belusko M, Liu M, Bruno F. Investigation of the effect of dynamic melting in a tube-in-tank PCM system using a CFD model. Appl Energy 2015;137:738–747. [CrossRef]

[57] Fornarelli F, Camporeale SM, Fortunato B, Torresi M, Oresta P, Magliocchetti L, et al. CFD analysis of melting process in a shell-and-tube latent heat storage for concentrated solar power plants. Appl Energy 2016;164:711–722. [CrossRef]

[58] Archibold AR, Gonzalez-Aguilar J, Rahman MM, Goswami DY, Romero M, Stefanakos EK. The melting process of storage materials with relatively high phase change temperatures in partially filled spherical shells. Appl Energy 2014;116:243–252. [CrossRef]

[59] Li WQ, Qu ZG, He YL, Tao WQ. Experimental and numerical studies on melting phase change heat transfer in open-cell metallic foams filled with paraffin. Appl Therm Eng 2012;37:1–9. [CrossRef]

[60] Agrawal KK, Misra R, Agrawal GD. CFD simulation study to evaluate the economic feasibility of backfilling materials for ground-air heat exchanger system. Geothermics 2021;90:102002. [CrossRef]

[61] Mihalakakou G, Santamouris M, Lewis JO, Asimakopoulos DN. On the application of the energy balance equation to predict ground temperature profiles. Sol Energy 1997;60:181–190. [CrossRef]

[62] Badescu V. Simple and accurate model for the ground heat exchanger of a passive house. Renew Energy 2007;32:845–855. [CrossRef]

[63] Khatry AK, Sodha MS, Malik MAS. Periodic variation of ground temperature with depth. Sol Energy 1978;20:425–427. [CrossRef]

[64] Zhang X, Xu M, Liu L, Yang Q, Song KI. Study on thermal performance of casing-type mine heat recovery device with phase change materials filling in annular space. Int J Energy Res 2021;45:1–20. [CrossRef]

[65] Hu P, Yu Z, Zhu N, Lei F, Yuan X. Performance study of a ground heat exchanger based on the multipole theory heat transfer model. Energy Build 2013;65:231–241. [CrossRef]

[66] Jalaluddin, Miyara A. Thermal performance investigation of several types of vertical ground heat exchangers with different operation mode. Appl Therm Eng 2012;33–34:167–174. [CrossRef]

[67] Kim D, Kim G, Kim D, Baek H. Experimental and numerical investigation of thermal properties of cement-based grouts used for vertical ground heat exchanger. Renew Energy 2017;112:260–267. [CrossRef]